Semi-active Attitude Control and Off-line Attitude Determination for the SEETI-Express Student Micro-satellite

Alminde, Lars

Publication date:
2005

Document Version
Publisher's PDF, also known as Version of record

Semi-Active Attitude Control and Off-line Attitude Determination for the SSETI-Express Student Micro-Satellite

Lars Alminde (*alminde@space.aau.dk*)*
Aalborg University, 9220 Aalborg E, Denmark

This paper concerns the development of the Attitude Determination and Control System (ADCS) for the SSETI-Express micro-satellite mission. The mission is an educational project involving 14 universities and the European Space Agency (ESA). The satellite has been designed and built, by students, over a period of only 18 months. This paper emphasises on the trade-offs required to build an operational ADCS system within such a rapid developing project.

Nomenclature

Unit Vectors	are written with a superscript hat, e.g. $\hat{n}$
Component vectors	are written in bold lowercase, e.g. $\mathbf{b}$
Matrices	are written with bold upper-case symbols, e.g. $\mathbf{A}$
Transformations	A transformation from frame x to frame y is denoted by: ${}^{\mathbf{x}}_{\mathbf{y}}\mathbf{A}$
Reference frames	indicated with superscripted prefix, ^{B} bodyframe and ^{I} inertial frame

Symbols

$\omega_{bi} = [\omega_x \omega_y \omega_z]^T$	satellite body rate vector
$\mathbf{A}$	General direction cosine matrix
$\mathbf{b}$	Magnetic field vector
$\hat{b}_x, \hat{b}_y, \hat{b}_Z$	Body frame unit vectors
$\mathbf{J}$	Inertia matrix
$\mathbf{n}$	External acting forces vector
$\mathbf{n_d}$	External acting disturbance vector
$\mathbf{n_{mag}}$	External acting disturbance vector due to permanent magnet
$\mathbf{m}$	Magnetic moment vector
$\mathbf{m_{perm}}$	Magnetic moment vector for permanent magnet
T	Energy
$\mathbf{q}$	Attitude quaternion
$\mathbf{s}$	Sun vector
$\mathbf{x}$	state vector
$\hat{\mathbf{x}}$	estimated state vector
B_i	Intrinsic induction of magnetic material $[T]$
μ_0	Vacuum permeability $[4\pi \cdot 10^{-7}\ Tm/A]$

*PhD. student, Dept. of Control Engineering, Fredrik Bajers vej 7C, 9220 Aalborg E, Denmark

I. Introduction

In January 2004 a group of students met at the European Space Technology and Research Centre (ESTEC) in Holland to discuss the feasibility of building a micro-satellite, dubbed SSETI-Express, from parts derived from other student satellite projects, and launch it within one and a half year. The project is an initiative under the ESA education department and the Student Space Exploration and Technology Initiative (SSETI). The mission is managed and coordinated by the ESA Education Office and approximately 70 students organised in 14 groups from 9 universities in 8 European countries participate in the project.

The mission baseline has been to build the spacecraft around systems developed by students at local universities, emphasis has been put on systems which had already seen considerably development in order to be able to focus on system engineering and integration rather than subsystem development. From this basis a platform has been defined together with a number of payloads.

The design relies heavily on its sister project SSETI-ESEO (European Student Earth Orbiter), which is a much more complex satellite that has been developed by students since the year 2000 and is expected to launch in 2007. From the current SSETI-ESEO design SSETI-Express has derived the mechanical design, the Electrical Power System and the Propulsion System. It is a key objective of the mission to evaluate these systems prior to the launch of ESEO. The envelope of the SSETI-Express satellite is 60x60x80 cm and 62 kg.

The AMateur SATellite organisation (AMSAT) supplies both an UHF band as well as a S-band radio for the satellite. These can be used separately as telemetry and tele-command transceivers, or be combined to act as a voice transponder as a service to the radio amateur community.

In addition the satellite carries a small camera, which will be able to take colour pictures of the Earth as well as celestial targets. The camera is the original engineering model from the AAU-Cubesat project.[1]

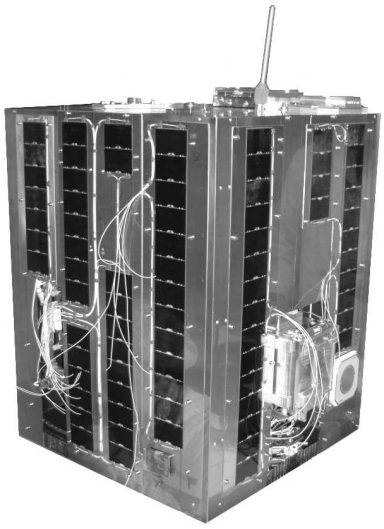

Figure 1. SSETI-express photographed during final integration

Finally the satellite itself carries three cubesat payloads which will be released from SSETI-Express satellite shortly after separation from the launch vehicle. A picture of the satellite during final integrations can be seen on figure 1

The system definition phase lasted throughout the spring of 2005 and was conducted as a spiraling process with increasing level of refinement. The phase was facilitated by weekly meetings using Internet Relay Chat (IRC), newsgroups for detailed discussions, and two intensive workshops were participants had the chance to discuss face-to-face.

In parallel the individual teams worked hard to refine and mature the hardware and software systems. For some subsystems it was impossible to find suitable hardware which had already seen considerable development; therefore also a few complete new developments were undertaken.

Starting in the early summer of 2004 subsystems have been delivered to ESTEC where the integration effort has been an on-going incremental process until March 2005 from whence system level testing has been

the major activity. The integration work has primarily been supported by the teams sending people to ESTEC to perform the work under close supervision from the project coordinator of the ESA Education Office.

One of the major design gabs was the Attitude Control and Determination System (ADCS), where no available systems could be adopted within time. This article describes the subsequent development of an ADCS system for SSETI-Express, which from specification to delivery was finished in 10 months. The system described in this paper provides a minimalistic ADCS system that meets all the operational requirements and has been developed under continuous coordination with students from the other involved groups of the project.

A. Launch and Orbit

The SSETI-Express satellite is scheduled for launch on October the 27th 2005 atop a Russian Cosmos launch vehicle. The satellite will be injected into a 686km sun synchronous orbit with longitude of the ascending node at 10:30AM.

As one of the first autonomous operations, the satellite will commence detumbling in order to allow ground controller situated in Denmark to acquire the satellite and begin the commissioning phase.

B. Requirements, Design Overview and Paper Organisation

During the conceptual design phase of the project, the following functional requirements for the ADCS systems were formulated. The ADCS system must:

1. be able to detumble the satellite following launch
2. ensure compatible antenna pointing for communication with ground stations in North Europe
3. ensure camera pointing that allows images to be taken of Europe
4. provide three-axis attitude determination with best efforts requirements in support of payload operations

This has led to the design of two decoupled systems for control and determination respectively. This means that the designed control system operates without attitude knowledge. This functionality has been obtained using a mix of permanent magnets and electro-magnetics coils controlled from magnetometer feedback as will be described fully in section II.

The attitude determination part of the system relies on data from an on-board magnetometer and two vector sun-sensors. These data are recorded by the telemetry system on the satellite and then downlinked to the ground station, where the data are processed to provide attitude estimates using a Kalman filtering approach as described in section III. The reliance on off-line determination was made possible as no other system on-board the satellite requires real-time attitude estimation. The final section, see section IV will provide concluding remarks.

II. Attitude Control Strategy

The attitude control strategy relies on a permanent magnet mounted on the satellite to fix one axis of the spacecraft to the geomagnetic field of the Earth. This principle is depicted on figure 2. Here it can be seen that the satellite, represented by the bar magnet, will track the geomagnetic field lines of the Earth and hereby ensure that the "north pole" of the satellite will point roughly downwards when over the northern hemisphere.

This pointing has been found sufficient to met the pointing requirements described in section B. However, to ensure that there is no excess rotational kinetic energy stored in the satellite inertia then the system is augmented with two electromagnetic coils that will be controlled actively to dissipate any excess energy. Specifically this will be important in the detumbling phase, following separation from the rocket, where there may be high angular velocities due to the separation from the launcher upper-stage.

The resulting configuration of the two coils and the permanent magnet can be seen on figure 3. It is important to note that this system will not be able to control the rotation around the $\mathbf{b_z}$ axis. However, due to gyroscopic coupling then any angular rate around this axis will transfer energy to the other two degrees

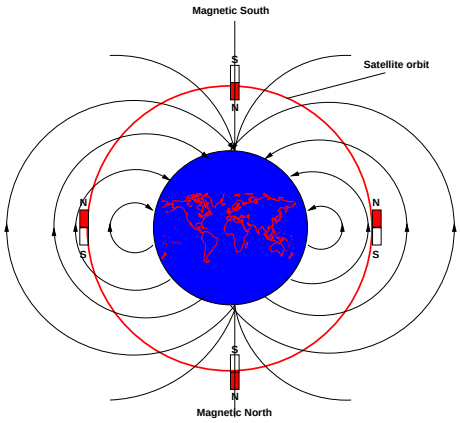

Figure 2. Attitude Control with permanent magnet

of freedom, which are controllable. It is therefore expected that there will be a very slow residual rotation around the $\mathbf{b_z}$ axis and the thermal design of the satellite has been designed to cope with this. Situation.

The next subsections will concisely describe the theory behind the control systems, its implementation and provide key simulation results.

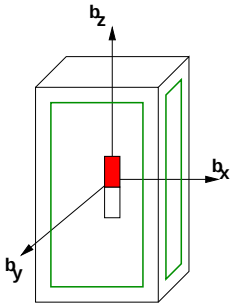

Figure 3. Configuration of passive and active actuators

A. Theory and Design

In the following some important points from the design process of this control system are presented. Specifically with regard to dimensioning the passive magnet and with regards to the control law for energy dissipative control.

1. Design of Passive Magnet

It was found using iterative simulations that a permanent magnet providing a magnetic moment of 5 Am^2 would be sufficient to meet the requirements pointing without jeopardizing constraints from the launch provider and other on-board systems for magnetic field strengths.

In order to calculate the volume of a permanent magnet of a certain magnetic material that will provide the equivalence of 5 Am^2 the following formula can be utilized:[2]

$$m_{perm} = \frac{B_i V}{\mu_0}[Am^2] \tag{1}$$

For the material Neodymium (N35) this corresponds to a magnet in the form of a cube with sides being 29 mm. The best fit commercially available magnet found was a make solution of four stacked cylindrical Neodymium (N35) magnets with a diameter of 18 mm and thickness of 6 mm each, providing an equivalent magnetic moment of 5.67 Am^2.

2. Active Energy Dissipation

As described in section B, a controller that makes the satellite expel excess kinetic energy is required in order to detumble the satellite and keep it aligned with the geomagnetic field without librations around the field lines. This type of control can be implemented using the "B-dot" control law which has flight heritage from e.g. the Ørsted[3] and PROBA[4] satellites, where it in both cases was used successfully for detumbling and contingency mode control. The control law formulated in the body-frame is given by:

$$^{\mathbf{B}}\mathbf{m_{ctrl}} = -\mathbf{k}^{\mathbf{B}}\dot{\mathbf{b}} \tag{2}$$

It generates a magnetic moment using the on-board electromagnetic coils that is negatively proportional to the derivative of the magnetic field as measured in the body-frame. This derivative will be sensitive to two things; the body rates of the satellite and the curvature of the geomagnetic field as the satellite traverses its orbit. In effect the algorithm will dissipate energy down to a level corresponding to the rotation of $4\pi/orbit$ meaning that the satellite will track the geomagnetic field.

To analyze stability then not only equation 2 should be considered, but also the contribution from the permanent magnet, which also provides control torques. Including this, the control law becomes:

$$^{\mathbf{B}}\mathbf{m_{ctrl}} = -\mathbf{k}^{\mathbf{B}}\dot{\mathbf{b}} - ^{\mathbf{B}}\mathbf{m_{perm}} \tag{3}$$

where:
$\mathbf{m_{perm}}$: is the constant magnetic moment provided by the permanent magnet, $\mathbf{m_{perm}} = [0\ 0\ 5.67]^T\ [Am^2]$

Lyapunov's first method can now be applied to show that the controller in fact dissipates energy, i.e. the derivative of the energy function is negative semi-definite (Following based on[3]). The energy of the satellite can be expressed as:

$$T = \frac{1}{2}\omega_{\mathbf{bi}}^{\mathbf{T}}\ ^{\mathbf{B}}\mathbf{J}\omega_{\mathbf{bi}} + \mathbf{m}_{\mathbf{perm}}^{\mathbf{T}}\ ^{\mathbf{B}}\mathbf{b} \tag{4}$$

Here the first term is the rotational kinetic energy of the satellite and the last term represents the potential energy of the satellite, which is proportional to the angle between the permanent magnet and the geomagnetic field and thus adequately described using the dot-product. The time derivative can be taken, using vector differentiation, as (noting that $\mathbf{J}\dot{\omega}_{\mathbf{bi}} = \mathbf{n_{ctrl}}$):

$$\dot{T} = \omega_{\mathbf{bi}}^{\mathbf{T}}\ ^{\mathbf{B}}\mathbf{n_{ctrl}} + \mathbf{m}_{\mathbf{perm}}^{\mathbf{T}}\ ^{\mathbf{B}}\dot{\mathbf{b}} \tag{5}$$

Inserting the control law yields:

$$\dot{T} = \omega_{\mathbf{bi}}^{\mathbf{T}}\ \left(-\mathbf{k}^{\mathbf{B}}\dot{\mathbf{b}} - ^{\mathbf{B}}\mathbf{m_{perm}}\right) \times ^{\mathbf{B}}\mathbf{b} + \mathbf{m}_{\mathbf{perm}}^{\mathbf{T}}\ ^{\mathbf{B}}\dot{\mathbf{b}} \tag{6}$$

To simplify this equation the following approximation of the derivative of the measured field is used:

$$^{\mathbf{B}}\dot{\mathbf{b}} = ^{\mathbf{B}}\mathbf{b} \times \omega_{\mathbf{bi}} + ^{\mathbf{B}}_{\mathbf{I}}\mathbf{A}\,^{\mathbf{B}}\dot{\mathbf{b}} \simeq ^{\mathbf{B}}\mathbf{b} \times \omega_{\mathbf{bi}} \tag{7}$$

This equation shows that the derivative of the magnetic field as measured in the body frame depends on a term due to the rotational motion of the satellite and a term due to the rotation of the geomagnetic field as the satellite traverses its orbit. If the satellite is tumbling then it is assumed that the body rates is much higher than the rate of the geomagnetic field, and the approximation as indicated by the last equal sign is valid. Inserting this result into equation 6 yields:

$$\dot{T} \simeq -\mathbf{k}^{\mathbf{B}}\dot{\mathbf{b}}^{\mathbf{T}}\ ^{\mathbf{B}}\dot{\mathbf{b}} - ^{\mathbf{B}}\mathbf{m}_{\mathbf{perm}}^{\mathbf{T}}\ ^{\mathbf{B}}\dot{\mathbf{b}} + \mathbf{m}_{\mathbf{perm}}^{\mathbf{T}}\ ^{\mathbf{B}}\dot{\mathbf{b}} = -\mathbf{k}^{\mathbf{B}}\dot{\mathbf{b}}^{\mathbf{T}}\ ^{\mathbf{B}}\dot{\mathbf{b}} \tag{8}$$

Clearly, this equation is negative semidefinite as long as the **k**-vector is negative in all terms, meaning that proper control gains to ensure energy dissipation can be implemented. However, some approximation was needed in order to derive this result and the interpretation of this approximation is that the algorithm does not provide inertial velocity stabilization, but rather stabilization to the rate of the geomagnetic field lines as seen in the body frame when orbiting the Earth.

In this specific case where only two electromagnetic coils are available then the gain vector will have zero gain for the $\hat{b}_z$-axis, but this does not qualitatively change the above result, as energy is still either maintained or expelled, but never increased.

B. Implementation

The following provides some details on the implementation of the attitude control system.

1. *Electromagnetic Coils*

The two electromagnetic coils mounted on the sides of SSETI-Express, has been made from isolated cobber wire wound in loops and glued to the sides of the satellite structure. The coils are driven by simple power electronics that only allows the coils to be on or off with the current flowing in either direction. The maximum magnetic moment that can be applied by each coil is $5Am^2$.

2. *B-dot Control Law*

The control law has been implemented on the on-board computer according to the block diagram presented in figure 4.

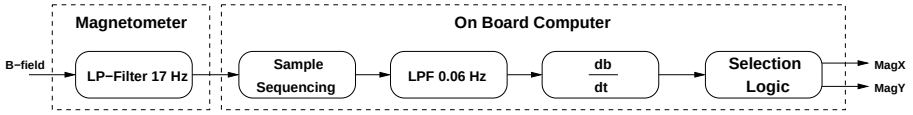

Figure 4. Block diagram of the B-dot implementation

Operation of the coils will affect the magnetic field as measured by the magnetometer therefore the "sample sequencing" block in the diagram alternates between periods where the coils are used and periods where measurements are obtained. The alternating frequency is 6 Hz.

The sampled data from the magnetometer is low-pass filtered and then a numerical estimate of the derivative is calculated and a decision on coil actuation is the taken. In order to conserve power then the absolute field derivative must be higher than 12 nT/s for the coils to become active. However, this value is adjustable by tele-commands.

C. Simulation Results

The design has been verified through simulation using Matlab/Simulink. The following will provide results for geomagnetic field tracking and detumbling situations. The simulation models include the satellite attitude dynamics, kinematics and the following environmental disturbance torques: Gravity gradient, residual atmospheric pressure and solar radiation pressure.

1. *Tracking Performance*

For the first scenario the satellite is initially at rest and closely aligned with the geomagnetic field. 6 orbits is simulated and the tracking of the field lines is investigated. The results are shown in figure 5.

The (TOPLEFT) figure show the absolute pointing error with regard to the geomagnetic field-lines, taken from the dot-product between the $\hat{b}_z$ vector and the geomagnetic field vector in the ECI frame. It can be seen that the tracking error is under 5 degrees after the initial large deviation where the satellite spins up from zero velocity to a velocity corresponding to the average rotation rate of the geomagnetic field.

Further, it can be seen that the error peaks at full and half fractions of orbits, which is due to the fact that the satellite at these times pass over the equator region where the curvature of the geomagnetic field is at its highest, and it is therefore more difficult for the satellite to track the field. Over the polar regions where pictures are to be taken the error is typically less than 1 degree.

The (TOPRIGHT) figure is the applied control moment during the simulation after being low-pass filtered at 0.01 Hz. Again it can be seen, apart from the initial control action, that the applied control moment is largest when passing the equator regions. The average magnitude of the applied control moment for each electromagnetic coil over the complete simulation is $\simeq 0.22\ Am^2$

The (BOTTOMLEFT) figure shows the norm of the body-rates and again it can be seen, as expected, that it peaks over the equatorial regions. And the average velocity throughout the period corresponds to the $4\pi/orbit \simeq 0.0021\ rad/s$

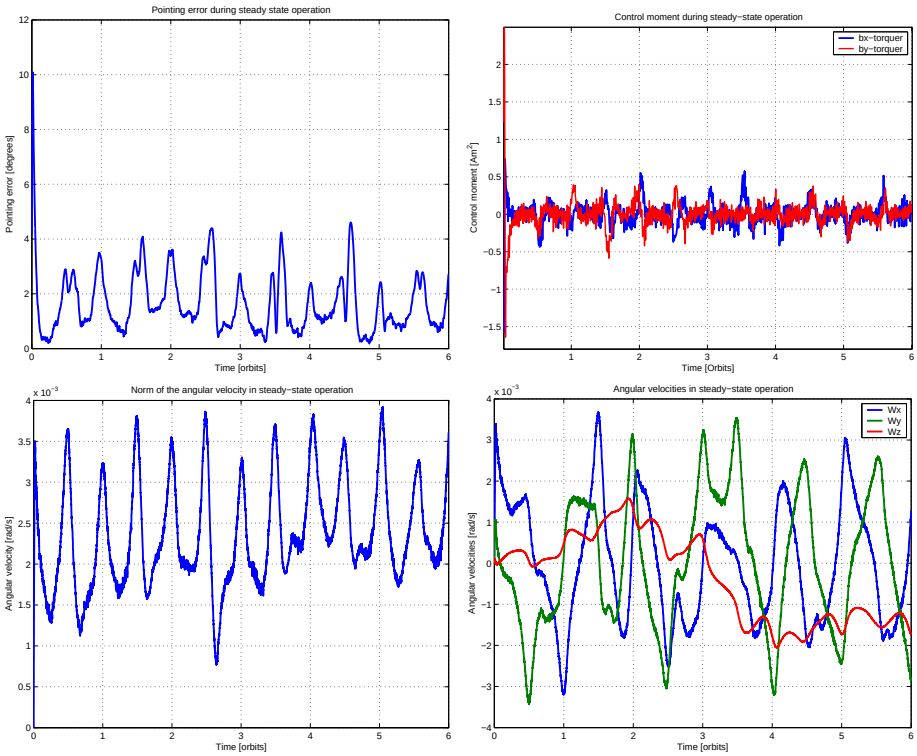

Figure 5. TOPLEFT: Absolute pointing error. TOPRIGHT: Magnetic control moment. BOTTOMLEFT: Norm of body-rates. BOTTOMRIGHT: body-rates

The (BOTTOMRIGHT) figure shows the body-rates throughout the simulation. The $\hat{b}_x$ and $\hat{b}_y$ rates follows the expected pattern and show high angular velocities over the equatorial regions. The $\hat{b}_z$-axis which is not affected directly by the control action exhibits different behavior and seems to switch between rotating slowly first in one direction and then the other.

2. Detumbling

In order to verify that the satellite is able to detumble the satellite a scenario is presented where the satellite initially has body rates of $[\omega_x\ \omega_y\ \omega_z] = [8\ -7\ 1]$ $degrees/s$ (norm is 10.67 $degrees/s$), i.e. worst case tumble scenario. Most of the angular velocity is placed on the $\hat{b}_x$ and $\hat{b}_y$ axes as the separation mechanism (ASAP5) is most likely to induce angular velocities around theses axes. The results are shown in figure 6.

From the pointing error (TOPLEFT) it can be seen that the satellite tumbles for approximately 2.5 orbits before the attitude is acquired and thereafter the pointing error evolves as shown for the previous steady-state scenario.

From the applied magnetic control moment (TOPRIGHT) it is clear that maximum control effort is used in order to detumble the satellite until the rotation reduces to a level corresponding to the rotation of the geomagnetic field during the orbit.

The norm of the velocity (BOTTOMLEFT) again shows the detumbling sequence, but it can also be seen that after acquisition the velocity continues to decay slowly. This is because the satellite ends up in an uncontrolled spin about the $\hat{b}_z$-axis that only decays very slowly, as can be seen from the (BOTTOMLEFT) figure, as the momentum is transfered away from the $\hat{b}_z$-axis by the nonlinear attitude dynamics.

This momentum transfer mechanism is also evident from the (BOTTOMRIGHT) figure during tumbling where the momentum transfer can be seen to cause rapid variation between the angular velocities between the three axes.

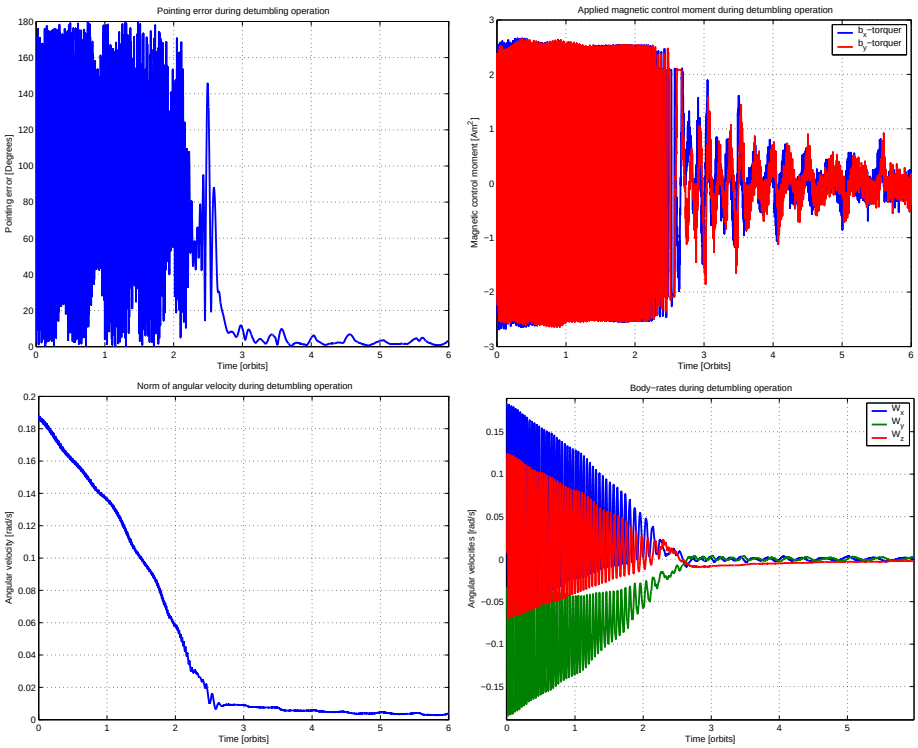

Figure 6. TOPLEFT: Absolute pointing error. TOPRIGHT: Magnetic control moment. BOTTOMLEFT: Norm of body-rates. BOTTOMRIGHT: body-rates

D. Conclusion on Attitude Control

The proposed control scheme consisting of a mix between passive and active means has shown itself to be adequate to the job of detumbling the SSETI-Express satellite and keeping the camera axis aligned with the geomagnetic field in order to provide an attitude that supports communication and photographing over the northern hemisphere.

The inclusion of the permanent magnet helps to keep a low power budget for the ADCS system, and it provides some degree of control in periods where the ADCS system is not powered. In fact eddy-currents in the satellite, ferromagnetic materials and structural flexibility provides a secondary mechanism for power dissipation, however, modeling of these secondary dissipative effects have, been beyond the scope of this work.

By adding measurements of the static power usage from the magnetometer and power electronics with the simulated power expelled in the coils then power budget for the ADCS system has been estimated roughly 100 mW when detumbled.

III. Attitude Determination Strategy

The attitude determination strategy calls for measurements from the on-board magnetometer and sun-sensors to be downlinked to ground where the attitude is reconstructed using recursive filtering. The following will provide details on the sensors generating the measurement and provide an overview of the filter structure that has been used. Lastly, simulation results will be presented for the attitude determination performance.

A. Sensors and Observeability

The following will describe the chosen sensors and the observeability that they together will provide.

1. Magnetometer

The commercially available of the shelf HMR2300[5] magnetometer from Honeywell has been chosen for the SSETI-express mission with some modifications performed in order for it to be more robust in the space environment. The magnetometer is mounted such that the sensitive axes of the instrument is aligned with body-frame of the satellite. The following table provides the error-budget for the magnetometer:

Error source	**RMS (nT)**	**RMS (degrees)**
Magnetometer white noise	17.9	0.068
Magnetometer linearity/gain error	240	0.92
IGRF model error (order 10)	100	0.38
In track error (SGP4 and timesync) 18km	76	0.29
Total	444	1.63

The sensor is assumed to exhibit negliable misalignment errors due to its favorable mounting position directly on the load bearing structure, and due to the mechanical interface that provides for good mounting accuracy.

2. Two-Axis Sun-Sensors

For this project two two-axis sun sensor are employed. These are spare sensors from the DTUsat cubesat project undertaken at the Danish Technical University (DTU). The sensors have a field of view of $\pm 70^o$ and provides outputs proportional to the lateral and horizontal angle to the sun, further a reference area on the chip is used to linearize the output and increase output insensitivity to temperature.[6] The sensors are respectively mounted on the X+ and X- panels of the satellite. The following table provides the error-budget for the sun-sensors:

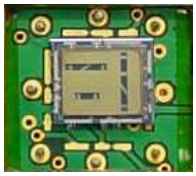

Figure 7. Sun-sensors from DTU

Error source	**RMS (degrees)**
Sun-sensor white noise	0.08
Ephemeris model error	0.003
In track error (SGP4 and timesync) 18km	0.007
Total	0.09

The sun-sensor RMS error is clearly very small and it is expected that the misalignment due to mechanical mounting will dominate the attitude determination error introduced by the sun-sensors. The misalignment error is expected to be less than a half degree.

3. Practical Observeability in the SSETI-Express Orbit

As demonstrated by the Ørsted satellite then it is under certain conditions possible to do three-axis attitude estimation using only a magnetometer.[7] However, on SSETI-express where the Z-axis of the satellite will point along the magnetic field lines, rotation around the field lines is not observable from the magnetometer alone, and the sun-sensors do not provide omni-directional coverage due to their limited field of view.

This means that there will be periods where 3-axis attitude determination cannot be expected, namely during eclipse, but also in the situation where the sun-vector and magnetic field vector are close to collinear. Figure 8 provides a rough sketch of the observeability situation in the near noon-midnight orbit of SSETI-express.

At the positions marked with the green arrows on figure 8 the sun-vector and magnetic field vector will be nearly collinear. These are also the positions where the sun can be expected to be outside the field of view of the sun-sensors.

B. Extended Kalman Filtering

The topic of Extended Kalman Filtering (EKF) for attitude reconstruction from magnetometer and sun-sensor data is well described in literature and the details of the algorithm will not be presented here. See

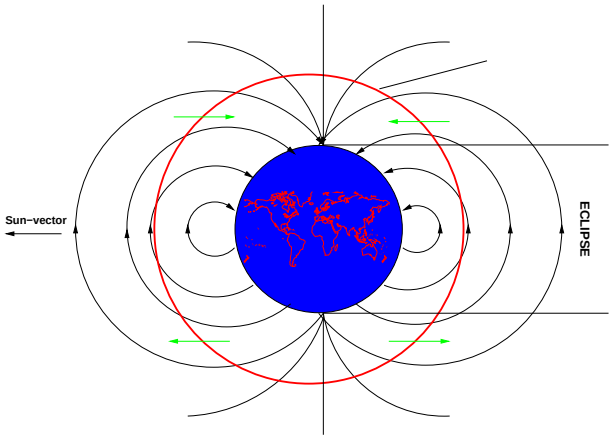

Figure 8. Sketch demonstrating practical observeability

e.g.[7] for more information. However, this section will describe what model is used in the extended Kalman filter and what states are observed.

The model used for the dynamics of the satellite includes the gyro-scopic coupling, torque due to the permanent magnetic, and finally a vector of assumed constant disturbances (${}^{\mathbf{B}}\mathbf{n_d}$), which is estimated in the filter and describes the lumped effect of environmental disturbances as well as the unknown actuation from the b-dot control on-board the satellite[a]. The dynamical models is therefore stated as:

$$ {}^{\mathbf{B}}\dot{\omega}_{bi} = {}^{B}\ J^{-1}\left(-[\omega_{bi}\times]{}^{\mathbf{B}}\mathbf{J}\omega_{bi} + {}^{\mathbf{B}}\mathbf{n_{mag}} + {}^{\mathbf{B}}\mathbf{n_d}\right) \tag{9} $$

Further, the model then integrates the angular velocity in the kinematic model providing the attitude quaternion:

$$ \dot{\mathbf{q}} = \frac{\mathbf{1}}{\mathbf{2}}[\omega_{\mathbf{bi}}\times]\mathbf{q} \tag{10} $$

The full state being estimated by the EKF therefore consists of 10 elements grouped in 4 quaternion states, 3 angular velocities and 3 disturbance torques.

$$ \tilde{\mathbf{x}} = \begin{bmatrix} \mathbf{q_{bi}} \\ \omega_{\mathbf{bi}} \\ \mathbf{n_d} \end{bmatrix} \tag{11} $$

The noise models required for the EKF comes primarily from the presented sensor error budgets. The process noise is used as a tuning parameter for the filter; increasing process noise increases robustness and decreases accuracy, and visa versa for lowering the process noise. The process noise is introduced in the lowest derivative, i.e. the constant torques.

C. Attitude Estimation Results from Simulation

Here the performance of the filter will be evaluated using simulations. The filter operates with a sampling frequency of 1 Hz.Figure 9 shows the estimator performance for the attitude states represented by their Euler angles.

The simulated attitude is plotted with broken lines and it is clear from the (LEFT) graph that the only visible difference between the simulated and estimated attitude is during the eclipse, where there is a small yaw-lag in the estimation. Recall that the yaw states are not updated from measurements during the eclipse, but only propagated.

The (RIGHT) graph show the error of the estimate and the 2σ-bounds calculated from the covariance and using the small angle approximation of the quaternion vector part. The graphs show that there is a reasonable correspondence between the estimation error and the calculated covariance. Also the effect of entering the eclipse is clearly visible; the reduced observeability leads to higher uncertainty of the estimates.

[a]due to link budget constraints this information is not part of the telemetry

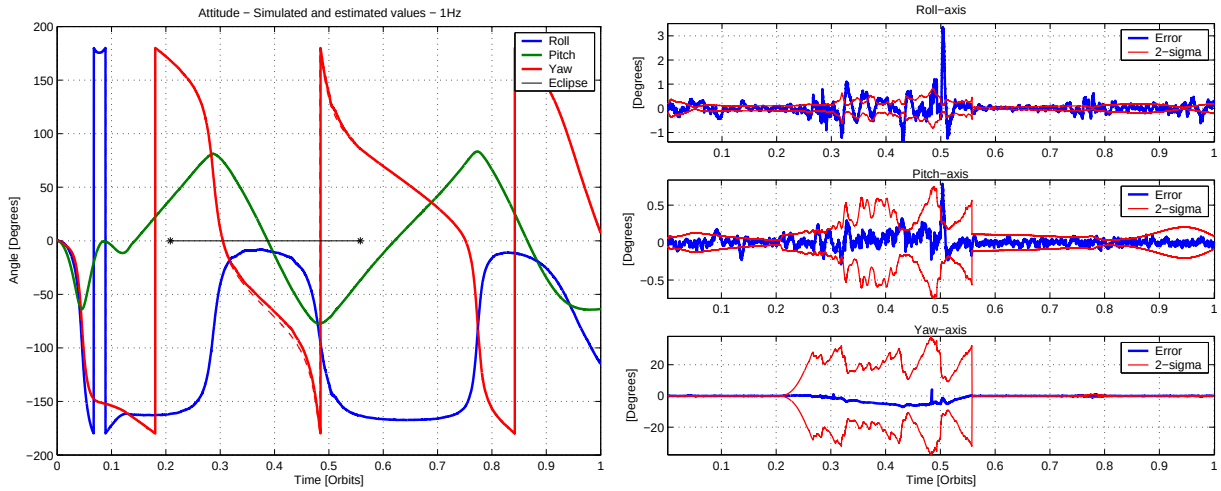

Figure 9. Performance of the EKF in terms of Attitude. Simulated and estimated Euler angles (LEFT). Estimation error and 2σ-bounds (RIGHT)

Figure 10 show the same results for the estimation of the angular velocities. Again it can be seen from the (LEFT) graph that the estimator tracks the state very well and deviations are only visible during the eclipse.

From the (RIGHT) graphs it is also clear that the estimation of the angular velocities is very accurate and the estimation error generally follows the pattern predicted by the covariance. Again it is seen that the uncertainty increases during the eclipse for all axes, and for the yaw axis in particular.

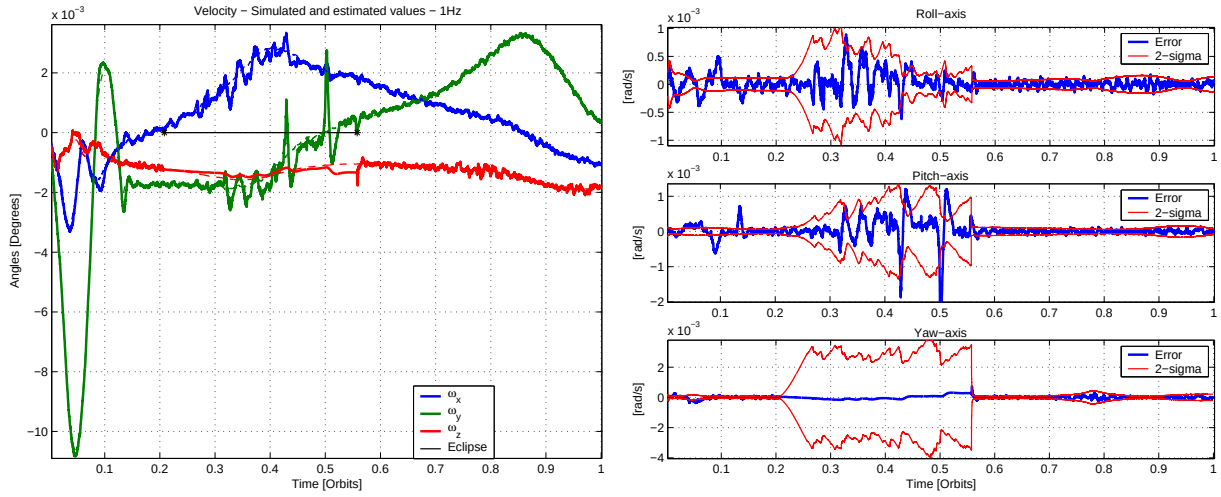

Figure 10. Performance of the EKF in terms of angular velocities. Simulated and estimated angular velocities (LEFT). Estimation error and 2σ-bounds (RIGHT)

Finally the results for the torque estimation are presented in figure 11. The (LEFT) graph show the estimated torques. Initially the large torques as the satellite aligns itself with the magnetic field is clearly visible, but then the signal is "lost" in the variance of the signal. This is a product of the fact that all the model uncertainty enters the process at this level, which gives relatively high Kalman gains for these states.

Therefore to demonstrate the estimators ability to estimate the torque states then a low-pass filtered version of the estimated state is shown on the (RIGHT) figure, and the stippled lines shows the sum of the disturbance and B-dot control torques from the simulator, which are also low-pas filtered[b] to remove the

[b] 4th order Butterworth, Fc=0.008 Hz

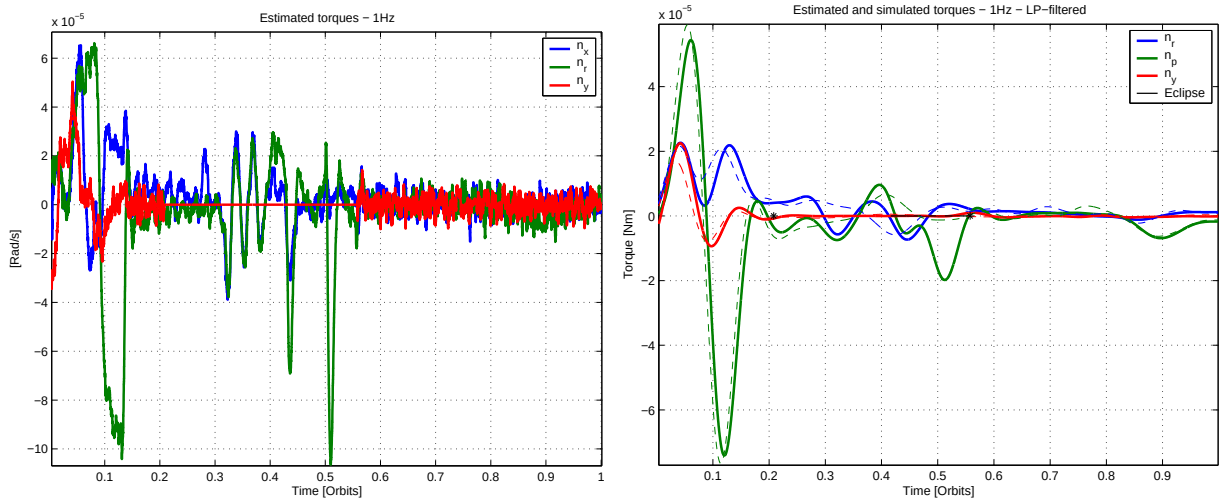

Figure 11. Performance of the EKF in terms of Torque Estimation. Estimated torques (LEFT). Filtered and compared to simulated (RIGHT)

switching spikes of the control torques. From the filtered graphs it is clear that there is a good correspondence between the estimated and simulated torques, except through the eclipse where discrepancies are clearly visible.

D. Conclusion on Attitude Determination

This section has provided an overview of the attitude determination system on SSETI-Express and demonstrated its abilities through simulations. Since all the software that implements the algorithms is situated and the ground station, rather than on the space-craft, then it is easy to make improvement over the course of spacecraft operations as more is learned about the in-orbit behaviour of the craft.

IV. Conclusion

This paper has provided an overview of the attitude control and determination system of the SSETI-Express together with simulations to show its expected performance. The paper has not included information on the important commissioning phase were e.g. the magnetometer bias, due to the presence of the permanent magnet, is to be estimated.

It is hoped that following a successful launch of the satellite then results gained from the flight data, including in-orbit paramter estimation results, can be presented.

References

[1]Alminde, L., Bisgaard, M., Vinther, D., Viscor, T., and stergaard, K. O., *AAU-Cubesat Architectual Overview and Lessons Learned*, IFAC, 2004, Proceedings of the 16th IFAC Symposium on Automatic Control in Aerospace, 2004, Sct. Petersburg, Russia.

[2]EMAGNETS, *Magnet Formulas*, www.netdenizen.com, 2004, www.netdenizen.com/emagnets.

[3]Wiesniewski, R., *Satellite Atittude Control Using Only Electromagnetic Actuation*, Aalborg University, 1996, PhD Thesis.

[4]Teston, F., Bernaerts, D., and Bermyn, J., *PROBA - Project for On-Board Autonomy*, ESA/ESTEC and Verhaert design, 1999.

[5]HONEYWELL, *Smart Digital Magnetometer - HMR2300*, Honeywell Inc., 2004, Downloadable from www.magneticsensors.com.

[6]Hales, J. and Pedersen, M., *Two-Axis MOEMS Sun Sensor for Pico Satellites*, AIAA, 2002, In proceedings of 16th Annual AIAA/USU Conference on Small Satellites.

[7]Bak, T., *Spacecraft Attitude Determination - a Magnetometer Approach*, Aalborg University, 1999, PhD Thesis.